ACS APPLIED MATERIALS & INTERFACES

Letter

www.acsami.org

Polydopamine Wrapping Silicon Cross-linked with Polyacrylic Acid as High-Performance Anode for Lithium-Ion Batteries

Yitian Bie,[†] Jun Yang,*[,†] Xiaolin Liu,[†] Jiulin Wang,[†] Yanna Nuli,[†] and Wei Lu[‡]

[†]School of Chemistry and Chemical Engineering, Shanghai Jiao Tong University, 800 Dongchuan Road, Shanghai, 200240, China

[‡]Department of Chemical Engineering, University of Michigan, Ann Arbor, Michigan 48109, United States

Supporting Information

ABSTRACT: A robust silicon electrode for lithium-ion battery has been developed via prepolymerizing dopamine on silicon particle surface and then chemical binding with poly(acrylic acid) (PAA). In this favorable electrode, silicon nanoparticles are covered by a thin layer of polydopamine (PD) through firm hydrogen bonds between phenolic hydroxyl and hydroxyl, while the elastic polymer layer reacts with PAA binder to form three-dimensional cross-linked binding system. The Si@PD/PAA electrode exhibits more stable cycle performance than conventional electrodes. In the case of thick electrode, a capacity of 3.69 mA h cm^{-2} and fairly good rechargeability for 80 cycles can be achieved.

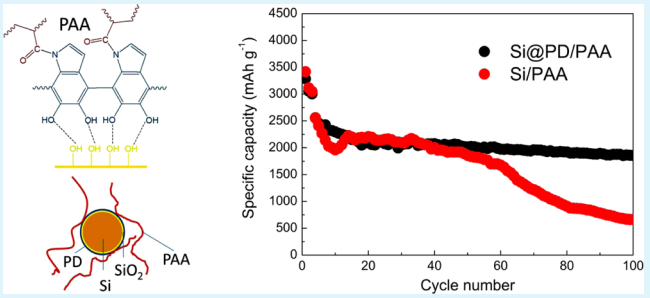

KEYWORDS: *silicon, binder, polyacrylic acid, dopamine, lithium-ion batteries*

As the essential component of electrodes, binder often has a great effect on the electrochemical performance,[1] especially for large-volume-change electrodes such as silicon, where binder could dominate the cycle stability. Many polymers have been studied as binders for silicon electrode, such as sodium carboxymethyl cellulose (CMC)[2−4] poly(vinyl alcohol) (PVA),[5] polyacrylonitrile (PAN),[6] polyimide (PI),[7] and sodium alginate (SA).[1] Poly(acrylic acid) (PAA)[8] has also been reported to be an advanced binder for Si-based anodes because of its high concentration of carbonyl groups, low swelling ability in carbonates and good elasticity. In addition, You Kyeong Jeong[9] first reported polymerized β-cyclodextrin (β-CDp) as binder for silicon electrode. In comparison to electrodes using SA and poly(vinylidene fluoride) (PVDF), electrode with β-CDp shows excellent cycle performance. The three-dimensional hydrogen-bonding interaction with Si particles provided by the hyperbranched network structure of β-CDp is responsible for the significant improvement.

Some methods have been employed to ameliorate the binder property.[10,11] Bonjae Koo[12] applied PAA and CMC simultaneously in silicon anodes and the cross-linked structure was effectively formed through the condensation reaction between them. Thus, the electrode showed better cycle performance. Wu Ming[13] synthesized a polymer binder with multifunctionality via introducing fluorenone, methylbenzoate ester groups, and triethylene oxide monomethyl ether side chains to polyfluorene type conductive polymers. The functional binder had high electronic conductivity, mechanical adhesion, ductility and electrolyte uptake. So far, most of studies on binders focused on the modification or synthesis of polymers.[14−18] However, because the electrode is an integration system, studying the electrode stability against the volume change from the three-dimentional configuration and the interaction between binder and other components is very important.[19,20]

Here we develop a simple and efficient silicon anode fabrication process via prepolymerizing dopamine on the silicon particle surface, which, in turn, conjugates to PAA binder in the electrode, as shown in Scheme 1. Investigations of the exceptional adhesion properties of mussel even on wet surfaces indicate that catechol, which is also contained in dopamine (Scheme 1a), plays a crucial role in the excellent wetness-resistant adhesion.[21,22] Complete polydopamine (PD) wrapping and firm hydrogen bonds between phenolic hydroxyl and hydroxyl can ensure a strong connection between silicon and the polymer elastic layer. Such a core−shell structure might suppress the Si particle pulverization. Moreover, the imino groups of polydopamine (PD) can react with carboxyl groups to cross-link PAA, thus forming a robust binding system in the electrode (Scheme 1b).

Figure 1a shows that the size of silicon nanoparticles is 50−200 nm. An amorphous SiO_2 (ca. 2 nm) layer covering on the surface of a silicon nanoparticle can be clearly observed in Figure 1b. After coated by PD, the amorphous layer increased to 3−4 nm (Figure 1c). It can be inferred that the particle is covered by a 1−2 nm layer of PD, which adhered to the SiO_2 surface firmly. According to the result of TGA tests in Figure 1d, there is ca. 5.8 wt % polymer in Si@PD nanoparticles. Such a thin layer of polymer might improve the mechanical

Received: November 4, 2015
Accepted: January 25, 2016
Published: January 25, 2016

DOI: 10.1021/acsami.5b10616
ACS Appl. Mater. Interfaces 2016, 8, 2899−2904

Scheme 1. (a) Chemical Structure of Dopamine; (b) Graphical Instruction of the Interaction between Different Components

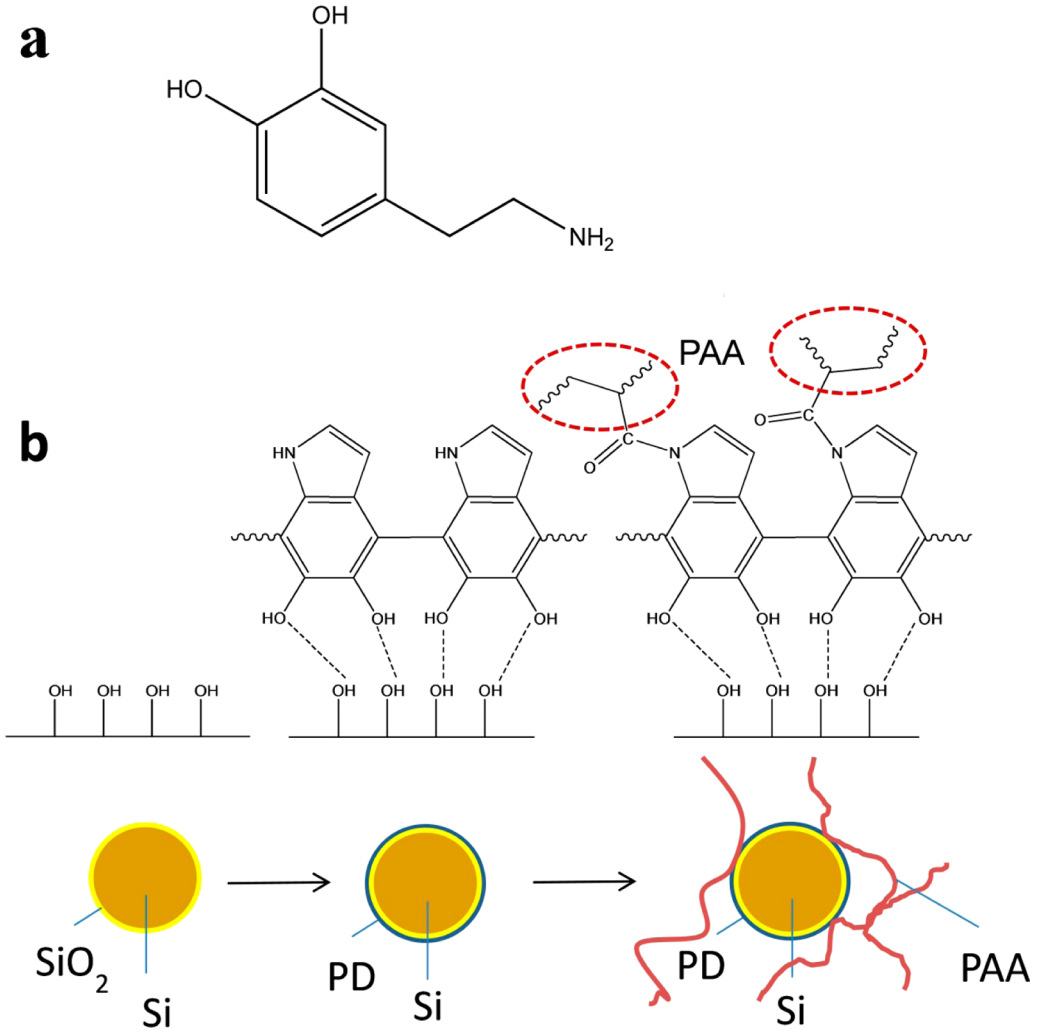

properties of the Si particles without hindering the electrical conduction.

FTIR spectroscopy confirms the existence of PD layer and the cross-linking reaction between PD and PAA. For Si sample in Figure 2a, the weak peak at 1627 cm^{-1} should correspond to O−H deformation vibration and the broad band between 1090 and 1180 cm^{-1} can be ascribed to Si−O stretching vibration, indicating that there is an oxide layer and a small amount of hydroxyl on the surface of silicon.[23] After wrapped by PD, the strong absorption at 1645 cm^{-1} is due to N−H deformation vibration of PD and other peaks at 1508, 1307, and 1221 cm^{-1} relating to C═C, C−N, and C−O vibrations also verify the PD layer.[24] In Figure 2b, the peak of N−H deformation vibration (1645 cm^{-1}) disappears in Si@PD/PAA electrode, suggesting that N−H in PD reacted with − COOH in PAA as shown in Scheme 1b. Moreover, deviation of the peak of C═O in PAA (1714 cm^{-1}) and Si@PD/PAA electrode (1700 cm^{-1}) also demonstrates that some carboxyl group in PAA has been transformed to amide. The electrode sample before 80 °C (i.e., drying naturally) shows a similar FTIR response to that after drying at 80 °C. It means that the reaction between PD and PAA might be easy to carry out under the solution state because they are alkaline and acid, respectively.

To further investigate the reaction between Si@PD and PAA, XPS measurements were also made on Si@PD particles and Si@PD/PAA electrode. N 1s regions of the two samples are shown in Figure 2c-d. For Figure 2c, the N 1s region of Si@PD particle is fit with two peaks assigned to primary ($-NH_2$) and secondary (−NH-R) amine functionalities.[24] And the N 1s spectrum of Si@PD/PAA electrode in Figure 2d exhibits an additional peak at 399.6 eV corresponding to tertiary amine (−NR−CO−).[24] The energies and assigned chemical groups for each peak and region scan for all elements detected are presented Figure S1 and Table S1. On the basis of the chemical structures of dopamine, PD and the electrode in Scheme 1, $-NH_2$ is associated with dopamine, −NH-R is associated with PD and -NR-CO- should be attributed to the condensation reaction between −NH-R in PD and −COOH in PAA.[24,25] We therefore conclude that covalent amide bond is formed between PAA and PD.

Figure 3 shows SEM images of electrodes with 2.0 mg cm^{-2} active materials loading before cycling. These high loading electrodes with relatively low percentage (10%) of binders have very high requirement on the mechanical properties of binders. Obviously, CMC cannot meet this requirement and the Si/CMC electrode exhibits numerous cracks (Figure 3a, b). In spite of the strong hydrogen bonds formed by the high concentration carboxyl in PAA, obvious cracks are also observed on Si/PAA electrode in Figure 3c, d. During the drying process, the surface tension of the liquid disappeared

DOI: 10.1021/acsami.5b10616
ACS Appl. Mater. Interfaces 2016, 8, 2899−2904

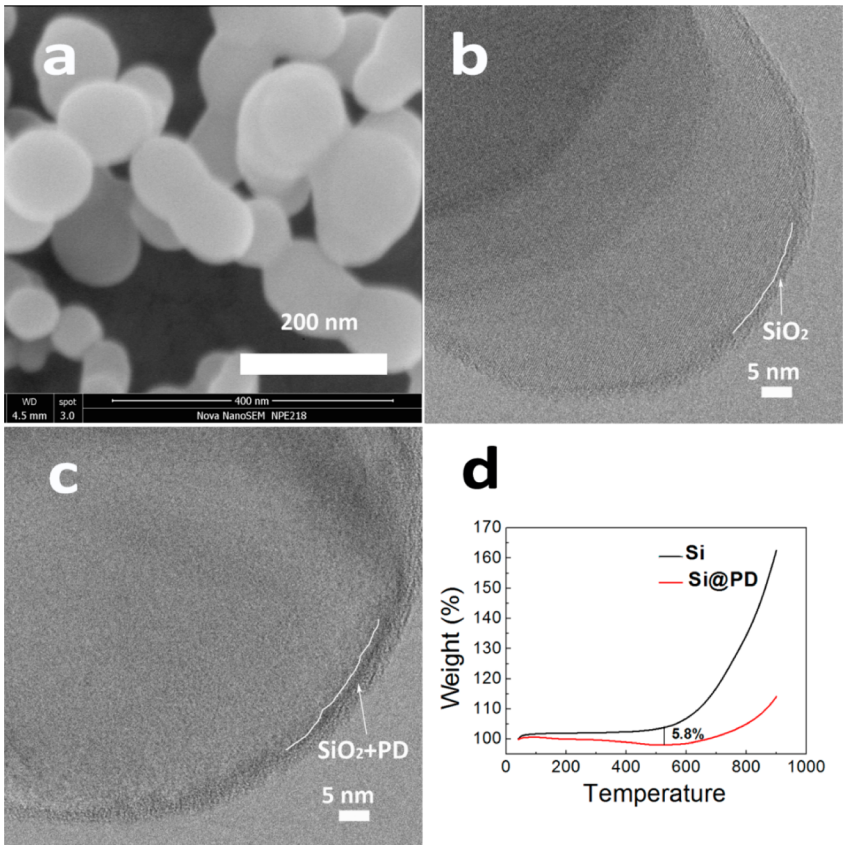

Figure 1. (a) SEM image of Si nanoparticles. (b) TEM image of Si nanoparticles. (c) TEM image of Si@PD nanoparticles. (d) TGA curves of Si@PD and Si.

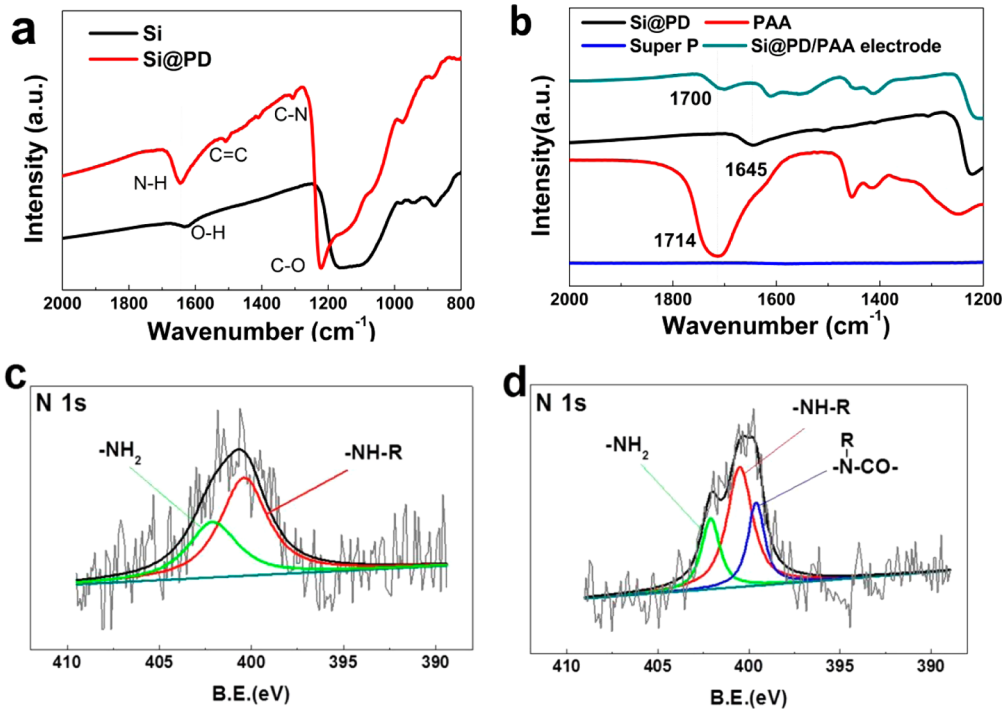

Figure 2. FTIR spectra of (a) nano Si and Si@PD, (b) Si@PD electrode and electrode materials. High-resolution XPS spectra of N 1s regions of (c) Si@PD particle and (d) Si@PD electrode.

with the solvent evaporation, which may lead to these cracks. Another important reason for cracking is that the binder strength is not strong enough. However, the Si@PD/PAA electrode remains intact in Figure 3e, f, because of the improved mechanic property of the binder after cross-linking[26] and the superior adhesion between silicon and binder.

DOI: 10.1021/acsami.5b10616
ACS Appl. Mater. Interfaces 2016, 8, 2899−2904

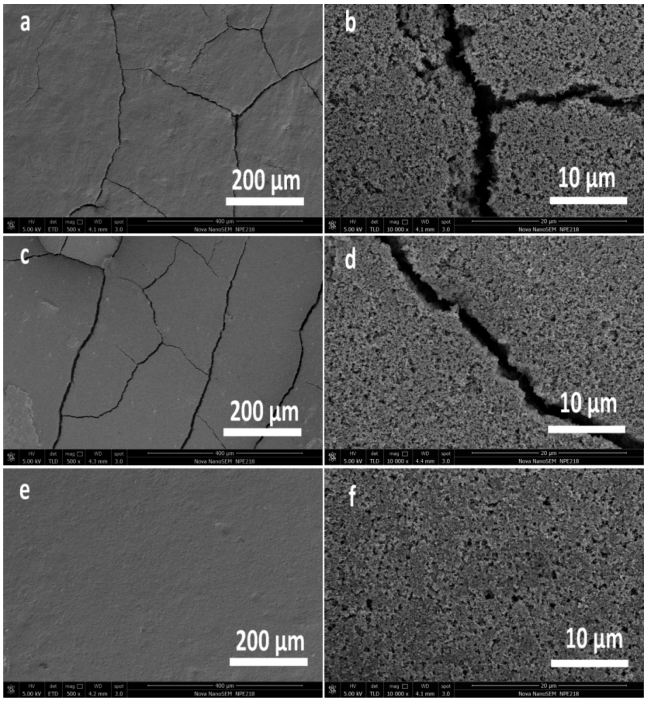

Figure 3. SEM images of (a, b) Si/CMC electrode, (c, d) Si/PAA electrode, and (e, f) Si@PD/PAA electrode before cycling.

Moreover, the peeling tests[10,27] were also conducted to evaluate the adhesion of the binders.(Figure S2) As shown in Table S2, the peeling force for Si@PD/PAA and Si/PAA electrodes are 0.614 and 0.561 N, indicating that the PD layer reinforces the connection between silicon and binder. The catechol groups in PD firmly attached to the surface of silicon while the imino groups in PD layer reacted with PAA and converted the two-dimensional linear binder to three-dimensional cross-linked binding system, providing superior mechanical properties for the electrode.

Figure 4a shows the cycle performance of Si@PD/PAA, Si/SA, Si/PAA, and Si/CMC electrodes with a loading of ca. 0.5 mg cm^{-2} active materials at 1.5 A g^{-1}. All the electrodes undergo fast capacity decay during the first several cycles caused by the structure degradation to a different extent and kinetics factor due to high current density. For Si/SA, the 10 percentages of SA cannot effectively stabilize the electrode structure, resulting in a low capacity of less than 1000 mA h g^{-1} after activation. In comparison, Si/CMC electrode can hold a higher capacity initially, but the capacity drops more quickly after 40 cycles. The Si/PAA electrode exhibits a similar cycling behavior to Si@PD/PAA in the initial stage. However, their difference gets apparent after 30 cycles. The fast capacity fading in the subsequent cycling stage indicates that the linear PAA binder cannot maintain a stable connection with silicon particles in the repeated enormous Si expansion/contraction process, which results in gradual loss of the electrical contact. The Si@PD/PAA electrode exhibits excellent cycle performance with a capacity of ca. 1800 mA h g^{-1} after 100 cycles while other electrodes show a capacity less than 800 mA h g^{-1}. It should be mentioned that Si@PD/PAA electrode also exhibits better cycle performance compared to Si/PAA electrode with 15% PAA, which contains same content of polymer. (Figure S3) On the other hand, SA and CMC binders belong to sodium salts. No effective interactions are established in the electrodes

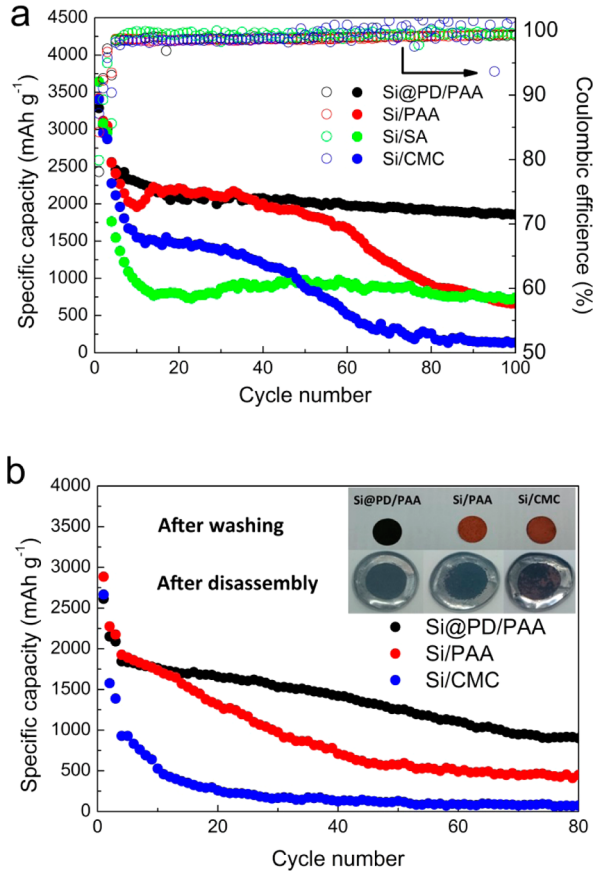

Figure 4. Cycling performance of Si@PD/PAA, Si/PAA, Si/SA and Si/CMC electrodes. The ration of Si or Si@PD, super P and binder is 8:1:1. (a) Active materials loading: ca. 0.5 mg cm^{-2}. Current density: 0.1 A g^{-1} for the first cycle, 0.3 A g^{-1} in the next two cycles, and 1.5 A g^{-1} for the following cycles. (b) Active materials loading: ca. 2.0 mg cm^{-2}. Current density: 0.1 A g^{-1} for the first cycle, 0.3 A g^{-1} in the next two cycles and 0.5 A g^{-1} for the following cycles. The inset image is the corresponding electrodes after 80 cycles.

due to the absence of sufficient −COOH groups and thus the cycle performance of Si@PD/SA and Si@PD/CMC cannot be improved in comparison with Si/SA and Si/CMC (Figure S4). However, their improvement is also possible, if the pH value of the slurries is adjusted carefully.

The rate performance of Si@PD/PAA and Si/PAA electrodes are compared in Figure S5. Apparently, Si@PD/PAA electrode shows higher cycle capacity than Si/PAA electrode for higher capacity at current density above 0.5 A g^{-1}, indicating that the strong adhesion of the ultrathin PD layer on silicon and the strong connection between PD and PAA do not influence the electrical conduction significantly, but enable the electrode excellent mechanical properties that can bear the volume change and maintain the whole electronic connection during cycling, thus contributing to the good cycle performance. In addition, the polymer layer might suppress fracture or pulverization of silicon particles, which often causes the electrical contact loss.

Figure 4b shows the cycle performance of Si@PD/PAA, Si/PAA, and Si/CMC electrodes with a loading of ca. 2.0 mg cm^{-2} active materials, which approaches the practical requirement. Even though the capacity fading becomes more serious for all electrodes, the superior binder function of Si@PD/PAA is further validated regardless of the electrode thickness. At the

DOI: 10.1021/acsami.5b10616
ACS Appl. Mater. Interfaces 2016, 8, 2899−2904

current density of 0.5 A g^{-1}, the Si/CMC electrode exhibits rapid capacity fade and its electrochemical activity is almost lost after 15 cycles while the Si/PAA electrode shows charge capacity of 1927 mA h g^{-1} at the first cycle and 1529 mA h g^{-1} is retained after 15 cycles. The difference can be attributed to the higher content of carbonyl groups in PAA, which can form hydrogen bonds and enhance the connection between silicon and binder. However, the low content of linear binders (10%) cannot hold the thick three-dimensional electrode structures for PAA. After 40 cycles, only 882 mA h g^{-1} remains for Si/PAA electrode, corresponding to 45% capacity retention. In contrast, the Si@PD/PAA electrode exhibits capacity of 1845 mA h g^{-1} at 0.5 A g^{-1}, corresponding to 3.69 mA h cm^{-2} at 1.0 mA cm^{-2} and 77% of the capacity can be retained after 40 cycles. After 80 cycles, its capacity is ca. 1000 mA h g^{-1}, much higher than those of others.

The charge and discharge curves of different electrodes are shown in Figure S6. Si@PD/PAA electrode exhibits fairly stable voltage trends after the fourth cycle at 0.5 A g^{-1}. In contrast, the charge and discharge platforms of Si/PAA and Si/CMC electrodes shift largely, indicating the aggravated voltage polarization during cycling caused by the structure degradation. Table1 further compares the Coulombic efficiencies of different electrodes in the initial 5 cycles. Although the first cycle efficiency of the thick Si@PD/PAA electrode is lower than that of the thin one (77.6% for 0.5 mg cm^{-2} loading), its advantage over other binder systems is still obvious. After the initial activation, its stable cycle efficiency reaches ca. 99.1%.

Table 1. Coulombic Efficiencies (%) Corresponding to Figure 4b

cycle	Si@PD/PAA	Si/PAA	Si/CMC
1	68.9	67.5	67.9
2	84.2	83.2	63.0
3	95.7	94.6	91.7
4	96.1	94.0	89.4
5	98.6	97.8	94.8

The inset image in Figure 4b shows the photos of the corresponding electrodes after 80 cycles. In the bottom of photos, only small amount of electrode material of Si/CMC attaches on Cu collector and the Si/PAA electrode also suffers from loss of the active material. After washing by polycarbonate (PC), only Cu foil stayed for Si/PAA and Si/CMC electrodes. In contrast, the Si@PD/PAA keeps the electrode morphology and shows no signs of fracture and pulverization. For Si/CMC and Si/PAA electrode, the interaction and connections between components are too weak to maintain the integrity during cycling and the silicon particles are divorced from the binder, leading to loss of the active material, whereas the binder system consisting of a sticky PD nanolayer and conjugated PAA can hold silicon particles together during the repeated expansion/contraction, and thereby stabilize the electrode structure.

To gain an insight of the interfacial property between electrode and electrolyte, we measured AC impedances and show nyquist plots of Si@PD/PAA and Si/PAA electrodes after the fourth cycle in Figure S7. This result confirms that the ultrathin PD layer does not enhance the interfacial resistance, but slightly accelerates electrochemical process.

In summary, a novel binding system has been developed for Si-based anode via prepolymerizing dopamine on the silicon particle surface and the followed conjugation to PAA. Complete and robust PD wrapping on Si and the cross-linking of PD and PAA reinforce the connection of silicon and binder and the mechanic properties of binder, which are favorable for the stability of the whole electrode structure. For Si@PD/PAA electrode, the capacity of ca. 1800 mA h g^{-1} is obtained at 1.5 A g^{-1} after 100 cycles while all other conventional electrodes show less than 800 mA h g^{-1} under the same condition. Additionally, its rate performance is improved. In the case of high loading, the Si@PD/PAA electrode achieves a capacity of 3.69 mA h cm^{-2} at 1.0 mA cm^{-2} and the electrode integrity can still be maintained after 80 cycles, differing from Si/PAA and Si/CMC electrodes, where crack, fracture, and detachment from Cu collector of the active layers take place.

■ ASSOCIATED CONTENT

Supporting Information

The Supporting Information is available free of charge on the ACS Publications website at DOI: 10.1021/acsami.5b10616.

Experimental details; XPS peak assignments; XPS spectra of all regions; results of peeling tests; photograph of the peeling test setup; cycle performance of Si@PD/PAA and Si/PAA electrodes with different amount of PAA; cycle performance and Coulombic efficiencies of Si@PD/SA, Si@PD/CMC, Si/SA and Si/CMC electrodes; The rate performance of Si@PD/PAA and Si/PAA electrode; charge and discharge curves of Si@PD/PAA, Si/PAA, Si/CMC electrode; Nyquist plots of Si@PD/PAA and Si/PAA electrodes (PDF)

■ AUTHOR INFORMATION

Corresponding Author

*E-mail: yangj723@sjtu.edu.cn. Tel./Fax: +86 2154747667.

Notes

The authors declare no competing financial interest.

■ ACKNOWLEDGMENTS

This work was supported by State Key 973 Program of the PRC (2014CB932303), SJTU-UM project, and China Postdoctoral Science Foundation (2015M581620).

■ REFERENCES

(1) Kovalenko, I.; Zdyrko, B.; Magasinski, A.; Hertzberg, B.; Milicev, Z.; Burtovyy, R.; Luzinov, I.; Yushin, G. A Major Constituent of Brown Algae for Use in High-Capacity Li-Ion Batteries. *Science* **2011**, *334*, 75−79.

(2) Buqa, H.; Holzapfel, M.; Krumeich, F.; Veit, C.; Novák, P. Study of styrene butadiene rubber and sodium methyl cellulose as binder for negative electrodes in lithium-ion batteries. *J. Power Sources* **2006**, *161*, 617−622.

(3) Bridel, J. S.; Azaïs, T.; Morcrette, M.; Tarascon, J. M.; Larcher, D. Key Parameters Governing the Reversibility of Si/Carbon/CMC Electrodes for Li-Ion Batteries†. *Chem. Mater.* **2010**, *22*, 1229−1241.

(4) Vogl, U. S.; Das, P. K.; Weber, A. Z.; Winter, M.; Kostecki, R.; Lux, S. F. Mechanism of Interactions between CMC Binder and Si Single Crystal Facets. *Langmuir* **2014**, *30*, 10299−10307.

(5) Park, H.-K.; Kong, B.-S.; Oh, E.-S. Effect of high adhesive polyvinyl alcohol binder on the anodes of lithium ion batteries. *Electrochem. Commun.* **2011**, *13*, 1051−1053.

(6) Shen, L.; Shen, L.; Wang, Z.; Chen, L. In Situ Thermally Cross-linked Polyacrylonitrile as Binder for High-Performance Silicon as Lithium Ion Battery Anode. *ChemSusChem* **2014**, *7*, 1951−1956.

(7) Kim, J. S.; Choi, W.; Cho, K. Y.; Byun, D.; Lim, J.; Lee, J. K. Effect of polyimide binder on electrochemical characteristics of

DOI: 10.1021/acsami.5b10616
ACS Appl. Mater. Interfaces 2016, 8, 2899−2904

surface-modified silicon anode for lithium ion batteries. *J. Power Sources* **2013**, *244*, 521−526.
(8) Magasinski, A.; Zdyrko, B.; Kovalenko, I.; Hertzberg, B.; Burtovyy, R.; Huebner, C. F.; Fuller, T. F.; Luzinov, I.; Yushin, G. Toward Efficient Binders for Li-Ion Battery Si-Based Anodes: Polyacrylic Acid. *ACS Appl. Mater. Interfaces* **2010**, *2*, 3004−3010.
(9) Jeong, Y. K.; Kwon, T.-w.; Lee, I.; Kim, T.-S.; Coskun, A.; Choi, J. W. Hyperbranched β-Cyclodextrin Polymer as an Effective Multi-dimensional Binder for Silicon Anodes in Lithium Rechargeable Batteries. *Nano Lett.* **2014**, *14*, 864−870.
(10) Ryou, M.-H.; Kim, J.; Lee, I.; Kim, S.; Jeong, Y. K.; Hong, S.; Ryu, J. H.; Kim, T.-S.; Park, J.-K.; Lee, H.; Choi, J. W. Mussel-Inspired Adhesive Binders for High-Performance Silicon Nanoparticle Anodes in Lithium-Ion Batteries. *Adv. Mater.* **2013**, *25*, 1571−1576.
(11) Han, Z. J.; Yabuuchi, N.; Hashimoto, S.; Sasaki, T.; Komaba, S. Cross-Linked Poly(acrylic acid) with Polycarbodiimide as Advanced Binder for Si/Graphite Composite Negative Electrodes in Li-Ion Batteries. *ECS Electrochem. Lett.* **2013**, *2*, A17−A20.
(12) Koo, B.; Kim, H.; Cho, Y.; Lee, K. T.; Choi, N.-S.; Cho, J. A Highly Cross-Linked Polymeric Binder for High-Performance Silicon Negative Electrodes in Lithium Ion Batteries. *Angew. Chem., Int. Ed.* **2012**, *51*, 8762−8767.
(13) Wu, M.; Xiao, X.; Vukmirovic, N.; Xun, S.; Das, P. K.; Song, X.; Olalde-Velasco, P.; Wang, D.; Weber, A. Z.; Wang, L.-W.; Battaglia, V. S.; Yang, W.; Liu, G. Toward an Ideal Polymer Binder Design for High-Capacity Battery Anodes. *J. Am. Chem. Soc.* **2013**, *135*, 12048−12056.
(14) Kwon, T.-w.; Jeong, Y. K.; Lee, I.; Kim, T.-S.; Choi, J. W.; Coskun, A. Systematic Molecular-Level Design of Binders Incorporating Meldrum's Acid for Silicon Anodes in Lithium Rechargeable Batteries. *Adv. Mater.* **2014**, *26*, 7979−7985.
(15) Park, Y.; Lee, S.; Kim, S.-H.; Jang, B. Y.; Kim, J. S.; Oh, S. M.; Kim, J.-Y.; Choi, N.-S.; Lee, K. T.; Kim, B.-S. A photo-cross-linkable polymeric binder for silicon anodes in lithium ion batteries. *RSC Adv.* **2013**, *3*, 12625.
(16) Liu, J.; Zhang, Q.; Wu, Z.-Y.; Wu, J.-H.; Li, J.-T.; Huang, L.; Sun, S.-G. A high-performance alginate hydrogel binder for the Si/C anode of a Li-ion battery. *Chem. Commun.* **2014**, *50*, 6386.
(17) Jeena, M. T.; Lee, J.-I.; Kim, S. H.; Kim, C.; Kim, J.-Y.; Park, S.; Ryu, J.-H. Multifunctional Molecular Design as an Efficient Polymeric Binder for Silicon Anodes in Lithium-Ion Batteries. *ACS Appl. Mater. Interfaces* **2014**, *6*, 18001−18007.
(18) Song, J.; Zhou, M.; Yi, R.; Xu, T.; Gordin, M. L.; Tang, D.; Yu, Z.; Regula, M.; Wang, D. Interpenetrated Gel Polymer Binder for High-Performance Silicon Anodes in Lithium-ion Batteries. *Adv. Funct. Mater.* **2014**, *24*, 5904−5910.
(19) Wang, L.; Wang, D.; Dong, Z.; Zhang, F.; Jin, J. Interface Chemistry Engineering for Stable Cycling of Reduced GO/SnO2Nanocomposites for Lithium Ion Battery. *Nano Lett.* **2013**, *13*, 6244.
(20) Wang, L.; Wang, D.; Dong, Z.; Zhang, F.; Jin, J. Interface Chemistry Engineering of Protein-Directed SnO2Nanocrystal-Based Anode for Lithium-Ion Batteries with Improved Performance. *Small* **2014**, *10*, 998−1007.
(21) Lee, H. K.; Lund, J. M.; Ramanathan, B.; Mizushima, N.; Iwasaki, A. Autophagy-dependent viral recognition by plasmacytoid dendritic cells. *Science* **2007**, *315*, 1398−1401.
(22) Lee, H.; Cheng, Y. C.; Fleming, G. R. Coherence dynamics in photosynthesis: Protein protection of excitonic coherence. *Science* **2007**, *316*, 1462−1465.
(23) Sun, C.; Deng, Y.; Wan, L.; Qin, X.; Chen, G. Graphene Oxide-Immobilized NH2-Terminated Silicon Nanoparticles by Cross-Linked Interactions for Highly Stable Silicon Negative Electrodes. *ACS Appl. Mater. Interfaces* **2014**, *6*, 11277−11285.
(24) Zangmeister, R. A.; Morris, T. A.; Tarlov, M. J. Characterization of Polydopamine Thin Films Deposited at Short Times by Autoxidation of Dopamine. *Langmuir* **2013**, *29*, 8619−8628.
(25) d'Ischia, M.; Napolitano, A.; Pezzella, A.; Meredith, P.; Sarna, T. Chemical and Structural Diversity in Eumelanins: Unexplored Bio-Optoelectronic Materials. *Angew. Chem., Int. Ed.* **2009**, *48*, 3914−3921.
(26) Lim, S.; Chu, H.; Lee, K.; Yim, T.; Kim, Y. J.; Mun, J.; Kim, T. H. Physically Cross-linked Polymer Binder Induced by Reversible Acid-Base Interaction for High-Performance Silicon Composite Anodes. *ACS Appl. Mater. Interfaces* **2015**, *7*, 23545−23553.
(27) Xu, Y. H.; Yin, G. P.; Ma, Y. L.; Zuo, P. J.; Cheng, X. Q. Simple annealing process for performance improvement of silicon anode based on polyvinylidene fluoride binder. *J. Power Sources* **2010**, *195*, 2069−2073.

DOI: 10.1021/acsami.5b10616
ACS Appl. Mater. Interfaces 2016, 8, 2899−2904